Comparative optical study of thulium-doped YVO_4, $GdVO_4$, and $LuVO_4$ single crystals

R. Lisiecki,* P. Solarz, G. Dominiak-Dzik, and W. Ryba-Romanowski
Institute of Low Temperature and Structure Research, Polish Academy of Sciences, Wrocław, Poland

M. Sobczyk
University of Wrocław, Faculty of Chemistry, Wrocław, Poland

Pavel Černý, Jan Šulc, and Helena Jelínková
Faculty of Nuclear Sciences and Physical Engineering, Czech Technical University, Břehová 7, Prague, Czech Republic

Yoshiharu Urata
Megaopto Co., Ltd, RIKEN Cooperation Ctr. W414, 2-1 Hirosawa, Wako, Saitama 351-0106, Japan

Mikio Higuchi
Graduate School of Engineering, Hokkaido University, Kita-ku, Sapporo 060-8628, Japan
(Received 15 March 2006; revised manuscript received 27 April 2006; published 7 July 2006)

$YVO_4:Tm^{3+}$ crystals grown by the Czochralski technique and $GdVO_4:Tm^{3+}$ and $LuVO_4:Tm^{3+}$ crystals grown by the floating-zone technique were investigated using methods of optical spectroscopy. Polarized absorption and emission spectra were recorded at room temperature and at 6 K. The crystal-field analysis was performed assuming the D_{2d} site symmetry for Tm^{3+} ions. In this way the missing crystal-field components of the $^3H_6$ ground multiplet were located. Room temperature absorption spectra were analyzed in the framework of the Judd-Ofelt theory. Evaluated radiative lifetimes of luminescent levels of Tm^{3+} follow a general trend diminishing in agreement with the sequence: $YVO_4:Tm^{3+} \rightarrow GdVO_4:Tm^{3+} \rightarrow LuVO_4:Tm^{3+}$. Luminescence lifetimes measured for the systems under study are similar except for the $^3F_4$ lifetime, which appears to be surprisingly short for $LuVO_4:Tm^{3+}$. Anisotropy of optical spectra is particularly pronounced in $LuVO_4:Tm^{3+}$. Peak absorption cross section for the band relevant for optical pumping at about 805 nm is roughly three times higher for π polarization. Stimulated emission cross sections for the $^3F_4$-$^3H_6$ transition near 1800 nm were evaluated using the reciprocity method. The diode-pumped continuous wave laser operation in $GdVO_4:Tm^{3+}$ with a slope efficiency of up to 40% is demonstrated. In $LuVO_4:Tm^{3+}$ the diode-pumped laser oscillation in a pulsed mode was observed.

DOI: 10.1103/PhysRevB.74.035103 PACS number(s): 42.55.Xi

I. INTRODUCTION

Single crystals of YVO_4 doped with neodymium were grown for the first time 40 years ago and their laser properties were then assessed.[1] It appeared that this crystal possesses an advantageous combination of desired features and may compete with commonly used YAG:Nd (yttrium aluminum garnet) crystals. In spite of this, the importance of $YVO_4:Nd$ lasers was marginal for decades because of serious problems encountered during the growth of YVO_4 crystals by the Czochralski method. An investigation of rare earth-doped YVO_4 crystals was, therefore, restricted to the area of basic research where the high crystal quality is not crucial. Numerous published papers reported on intensities of absorption and emission spectra and relaxation processes of excited states of rare earth ions in YVO_4 matrix.[2–6]

A breakthrough in the technology of YVO_4 crystal production, which occurred during the past decade, has been stimulated by the progress in the field of laser diodes. Emission of $Al_xGa_{1-x}As$ laser diodes around 808 nm with powers sufficient to pump neodymium lasers made it possible to take advantage of outstanding features of the $YVO_4:Nd$ system consisting of a broad and intense pump band and unusually high emission cross sections. Technological efforts were successful and laser quality crystals grown by the Czochralski method became available.

Following this achievement attention was directed towards thulium-doped YVO_4, because of its laser potential associated with the $^3F_4$-$^3H_6$ transition of Tm^{3+} ions near 1800 nm. The cw room temperature operation of the longitudinally pumped $YVO_4:Tm$ laser was reported.[7,8] Later, the thulium-doped $GdVO_4$ crystals were grown by the Czochralski method and their laser performance was examined.[9–11] In these early studies the optical pumping was provided by a Ti:sapphire laser, but quite recently the performance of a diode-pumped cw $Tm:GdVO_4$ laser with a slope efficiency of 28% and a maximum output power of 420 mW was reported.[12]

$Tm:LuVO_4$, to our knowledge, is the newest system. Its successful growth by a floating-zone technique was reported only recently.[13] Thus, thulium-doped vanadate crystals emerge as the most promising active media for diode-pumped all solid state lasers operating near 1.9 μm. The laser performance of these materials depend on parameters characterizing the source of optical pumping used, i.e., the Ti:sapphire laser or a laser diode, geometry of optical pumping and laser resonator. Properties of a laser active material are of paramount importance, however.

Knowledge on the spectral position and intensity of pump and emission bands, stimulated emission cross sections and relaxation dynamics of excited states makes it possible to predict the laser performance. It helps also to optimize the laser design.

Spectroscopic properties of $Tm:YVO_4$ crystals are well documented in published works.[14,15] Information on $Tm:GdVO_4$ is considerably poorer. In several published papers the attention was directed mainly to the laser performance of this system.[12] To our knowledge one published paper only deals with $Tm:LuVO_4$, reporting on the crystal growth process and preliminary spectroscopic data.[13] Intentions of the present work are as follows: (i) enrich the knowledge on fundamental spectroscopic properties of thulium-doped vanadate crystals; (ii) evaluate the effect of cation substitution $Y \rightarrow Gd \rightarrow Lu$ in the vanadate crystal structure on spectroscopic features; (iii) provide fundamental spectroscopic parameters relevant to the laser operation of these systems.

II. EXPERIMENTAL DETAILS

$Tm:YVO_4$ crystals were grown by the Czochralski method at the Institute of Electronic Materials Technology in Warsaw. Details of the growth process are given elsewhere.[16] Samples with nominal Tm^{3+} concentrations of 0.5 and 6 at. % were prepared. The actual Tm^{3+} concentration was slightly lower amounting to 0.46 and 5.6 at. % respectively, and is in agreement with the segregation coefficient for heavy rare earth ions in YVO_4.[16] $Tm:GdVO_4$ and $Tm:LuVO_4$ crystals were grown at the Hokkaido University in Sapporo by the floating-zone method employing the procedure described in Refs. 13 and 17. Samples of $GdVO_4$ with Tm^{3+} concentrations of 2, 4, and 6 at. % and samples of $LuVO_4$ with Tm^{3+} concentrations of 3 and 5 at. % were prepared for spectroscopic investigation. Uniform distribution of thulium ions in the crystal hosts was found indicating a segregation coefficient close to unity.[13]

Polarized absorption spectra were measured at 6 K and room temperature with a Varian model 5 UV-VIS-NIR spectrophotometer. The resolution was 0.5 nm in the visible range and 1 nm in the near infrared. Luminescence spectra were excited by an argon ion laser, dispersed by a 1-m double grating monochromator with a spectral bandwidth of 2 cm^{-1} and detected by a photomultiplier. The resulting signal was analyzed using a Stanford model SRS 250 Boxcar integrator and stored on a PC computer. Luminescence decay curves were recorded using a Tektronix model TDS 3052 digital oscilloscope. Short pulse excitation was provided by a continuum Surelite I optical parametric oscillator pumped by a third harmonic of a Nd:YAG laser. Samples were mounted in an Oxford model CF 1204 continuous flow liquid helium cryostat equipped with a temperature controller for a low temperature measurement of absorption and emission spectra.

III. RESULTS AND DISCUSSION

A. Crystal-field analysis

As far as we know the results of crystal-field analysis for $Tm:GdVO_4$ and $Tm:LuVO_4$ were not reported before. Those for $Tm:YVO_4$ appeared in several published works. The first analysis reported by Knoll[14] was made by using an operator equivalent technique. It did not describe the free ion adequately and in consequence different sets of parameters were consistent with different parts of spectrum. Wortman *et al.*[18] recalculated energy levels by using experimental data of Knoll and proposed a new interpretation of the $^3F_4$ and $^3H_5$ multiplets. More recently Chen Xueyuan and Luo Zundu carried out the crystal-field level fitting based on the analysis of the group-chain scheme for $Tm:YVO_4$.[15]

To perform the analysis for $Tm:GdVO_4$ and $Tm:LuVO_4$ the experimental energy levels were derived from polarized absorption spectra and from luminescence spectra associated with the $^1G_4$-$^3H_6$ and $^3H_4$-$^3H_6$ transitions, both recorded at 5 K. Additionally, we performed the analysis for $Tm:YVO_4$ using experimental data reported by Knoll in order to refer our approach to previous calculations.

In the D_{2d} crystal field the $(2J+1)$ degeneracy is partly lifted so, the J=0, 1, 2, 3, 4, 5, 6 levels split into 1, 2, 4, 5, 7, 8, 10 irreducible representations, respectively. The first crystal-field level of the $^3H_6$ ground state was assigned as Γ_5. Since the transitions observed at liquid helium temperature originate only from this level they must terminate on the Γ_5 for π polarization and Γ_1, Γ_2, Γ_3, Γ_4, for σ polarization.

Crystal-field calculations were performed by applying the *f*-shell empirical program of Reid (University of Canterbury, New Zealand) and running on PC under the Linux Lycoris Desktop LX operating system. The eigenvectors and eigenvalues of crystal-field levels were obtained by the diagonalization of the combined free-ion and crystal-field energy matrices. The complete Hamiltonian includes the following terms:

$$\hat{H} = \hat{H}_A + \hat{H}_{CF}. \tag{1}$$

The $\hat{H}_A$ contains the atomic parts of $\hat{H}$ and is defined as

$$\hat{H}_A = E_{ave} + \sum_k F^k \hat{f}_k + \alpha \hat{L}(\hat{L}+1) + \beta \hat{G}(G_2) + \gamma \hat{G}(R_7) + \zeta_{SO} \hat{A}_{SO} + \sum_k P^k \hat{p}_k + \sum_k M^k \hat{m}, \tag{2}$$

where E_{ave} is the spherically symmetric one-electron part in the Hamiltonian, $F^k(nf,nf)$ and ζ_{SO} represent the radial parts of the electrostatic and spin-orbit interaction, respectively, while $\hat{f}_k$ and $\hat{A}_{SO}$ are the angular parts of these interactions. The α, β, and γ parameters are associated with the two-body correction terms. $G(G_2)$ and $G(R_7)$ are Casimir operators for the G_2 and R_7 groups and L is the total orbital angular momentum. The M^k parameters arise from the spin-spin and spin-orbit interaction, while the P^k parameters represent the electrostatic spin-orbit interactions with higher configurations. The $\hat{H}_{CF}$ term of the Hamiltonian represents the one-electron crystal field and is defined as

$$\hat{H}_{CF} = \sum_{k,q,i} B_q^k C_q^{(k)}(i), \tag{3}$$

where $C_q^{(k)}(i)$ is a spherical tensor of a k rank and B_q^k are crystal-field parameters. The crystal field Hamiltonian for the D_{2d} site symmetry can be written as

$$H_{CF} = \sum_{k=2,4,6} B_0^k C_0^k + \sum_{k=4,6} B_4^k (C_4^k + C_{-4}^k). \tag{4}$$

One site only was observed for Tm^{3+}-doped MVO_4 (M = Y, Gd, Lu) in absorption and emission spectra and 48, 47, 44 levels for YVO_4, $GdVO_4$, $LuVO_4$ adequately. These experimental levels were fitted to the parameters of the phenomenological Hamiltonian. Free-ion and crystal-field parameters determined for Tm^{3+} in YVO_4 single crystals[15] were taken as initial values in our calculations. In the final fitting procedure six atomic free-ion parameters and five one-electron crystal-field parameters freely varied. Because of the limited data obtained for Tm^{3+}-doped orthovanadates, the β, γ, M^k, and P^k parameters were not varied, but held fixed at the values obtained for Tm^{3+}-doped LaF_3. The corresponding experimental and calculated energy values of the crystal-field levels are given in Table I. The complete parameters for both fits are presented in Table II. The σ standard deviations obtained for Tm^{3+} in $LuVO_4$, YVO_4, and $GdVO_4$ are close to the value of 13, 11, and 12 cm^{-1}, respectively.

The inclusion of the CCF parameters made it possible to decrease these Δ values as well as the rms deviation for the overall fitting (Table II). The crystal-field parameters obtained are consistent with the whole spectrum. Our rms deviation values are close to the 10.6 cm^{-1} value reported by Wortman *et al.*[18] but higher than 7 cm^{-1} to those reported for Tm:YVO_4 by Chen Xueyuan and Luo Zundu.[15] It should be noted, however, that in the latter calculation several data points were excluded from the fitting procedure.

A measure of the magnitude of the total crystal-field strength is given by the scalar parameter N_v, defined as

$$N_v = \left[(B_q^k)^2 \frac{4\pi}{(2k+1)} \right]^{1/2}. \tag{5}$$

A reliability of the crystal-field calculation performed can be further assessed upon inspection of Table III, which compares our B_g^k parameters for Tm:YVO_4 with those reported in aforementioned papers.[14,15,18] It can be seen that the values of the crystal-field parameters B_0^4, B_4^4, and B_4^6 obtained in the four approaches are much the same. Differences between values of the B_0^2 and B_0^6 parameters are slightly higher but still the agreement seems to be satisfactory. Accordingly, the physical significance of B_g^k parameters and their correlation with the structures of Tm:YVO_4, Tm:$GdVO_4$, and Tm:$LuVO_4$ can be discussed. In these crystal structures eight oxygen atoms coordinated by Tm^{3+} ions form dodecahedra with D_{2d} symmetry. The coordination number 8 is often observed in rare earth-doped crystals and literature dealing with this geometry is rich.[19–22] To derive a dodecahedron from a cube it is convenient to consider a cube as composed of two interpenetrating tetrahedra. Upon compression of one tetrahedron along the S_4 axis and an elongation of the other a dodecahedron will be formed. Within an approximation of the hard sphere model the shape of an ideal dodecahedron is characterized by angular coordinates of ligands $\theta_A = 36.9°$, $\theta_B = 69.5°$, and the ratio of radial distances from ligands to a central metal ion $R_A/R_B = 1$.[19] The algebraic sign of the B_g^k parameters is determined by their angular part, therefore, for an ideal dodecahedron, all B_g^k parameters, except for the B_0^2, would be negative. However, in real crystalline structures R_A/R_B may be as high as 1.08 and θ_A as low as 30°.[20] In our case the B_0^2 parameter is negative for the three systems studied. It indicates that one tetrahedron is compressed to a smaller extent than the other tetrahedron is elongated. This conclusion is consistent with results obtained during investigation of Eu^{3+} in vanadates. In particular, for Eu:YVO_4 $\theta_A = 32.83°$, $\theta_B = 78.10°$, and $R_A/R_B = 1.06$ has been reported.[20] The mean value of angles $\frac{1}{2}(\theta_A + \theta_B) = 55.47°$ is higher than $\theta_{cubic} = 54.74°$ and the B_0^2 parameter was found to be negative. It may be interesting to mention that in isostructural Eu:YPO_4 $\theta_A = 30.22°$, $\theta_B = 76.33°$, and $R_A/R_B = 1.03$. The mean value of angles amounting to 53.28° is smaller than θ_{cubic} and the B_0^2 parameter was found to be positive.[20] A prediction of signs of remaining crystal-field parameters is not straightforward, especially when R_A/R_B differs from unity. Nevertheless, taking into account the similarity of B_g^k parameter values and their algebraic signs, a general conclusion can be drawn that shape characteristics of dodecahedra around Tm^{3+} ions in YVO_4, $GdVO_4$, and $LuVO_4$ do not differ significantly.

B. Optical absorption spectra and the Judd-Ofelt treatment

Survey absorption spectra of thulium-doped YVO_4, $GdVO_4$, and $LuVO_4$ recorded at room temperature with light polarized perpendicular (π spectrum) and parallel (σ spectrum) to the optical axis of the crystal are compared in Fig. 1. In the three systems the matrix absorption rises steeply in the violet region of the spectrum but in YVO_4 it begins at much longer wavelengths. In addition, the steep absorption rise that forms a kind of edge is preceded in this crystal by a weaker absorption which increases monotonously with decreasing wavelength throughout the entire visible range. These findings indicate clearly that the YVO_4 host contains an appreciable density of point defects. The Tm:YVO_4 crystal was grown by the Czochralski method whereas two remaining systems were obtained by a floating-zone technique. Although the Czochralski method is expected to provide excellent quality crystals, the growth of vanadates is hampered by a loss of oxygen due to an instability of the oxidation state of vanadium in the melt. It appears that the floating-zone technique is more advantageous since it does not employ crucibles and crystals may be grown in an atmosphere of pure oxygen. However, the Tm:$GdVO_4$ and Tm:$LuVO_4$ crystals studied can, by no means, be considered as defect-free systems. It was pointed out in Ref. 13 that high oxygen partial pressure in a pure oxygen flow is effective in suppressing the evaporation of vanadium oxide, but not completely. After the growth of vanadate crystals, pale yellow precipitates (vanadium oxides) appeared on the inner wall of quartz tube, which protected the growth atmosphere from the

TABLE I. Electronic states, symmetry labels, experimental, and calculated energy levels (cm^{-1}) of Tm^{3+}-doped YVO_4, $GdVO_4$, and $LuVO_4$ single crystals.

Multiplet	Irrep.	YVO_4			$GdVO_4$			$LuVO_4$		
		E_{exp}[a]	E_{calc}	$E_{exp}-E_{calc}$	E_{exp}	E_{calc}	$E_{exp}-E_{calc}$	E_{exp}	E_{calc}	$E_{exp}-E_{calc}$
$^3H_6$	Γ_5	0	−4	4	0	−4	4	0	−10	−10
	Γ_1	54	30	24	57	27	30	52	36	16
	Γ_4	119	117	2		116			136	
	Γ_5	138	148	−10	134	136	−2		137	
	Γ_2	158	150	8		143		141	149	−8
	Γ_3	192	186	6	192	191	1		207	
	Γ_4	208	223	−15	214	216	−2	239	234	5
	Γ_1		313		303	295	8		301	
	Γ_5	332	348	−16	340	334	6	328	342	−14
	Γ_3		375			361		366	372	−6
$^3F_4$	Γ_4	5550	5558	−8	5548	5556	−8	5556	5565	−9
	Γ_5	5655	5656	−1	5648	5653	−5	5669	5669	0
	Γ_1	5723	5721	2	5704	5709	−5	5748	5742	6
	Γ_2	5775	5779	−4	5744	5744	−24	5782	5795	−13
	Γ_3	5825	5798	27	5764	5776	−14	5801	5781	20
	Γ_5	5860	5865	−5	5860	5850	10	5863	5862	1
	Γ_1	5879	5893	−14	5899	5886	13	5905	5913	−8
$^3H_5$	Γ_2	8204	8201	3		8199			8205	
	Γ_1	8232	8253	−21	8228	8248	−20	8242	8246	−4
	Γ_5	8268	8264	4	8265	8261	4	8276	8278	−2
	Γ_3	8296	8297	−1	8284	8288	−4	8304	8309	−5
	Γ_5	8338	8327	11	8314	8325	−11	8353	8340	13
	Γ_2	8440	8439	1	8408	8422	−14	8437	8441	−4
	Γ_5		8466		8448	8452	−4		8467	
	Γ_4	8491	8481	10	8465	8469	−4	8478	8482	−4
$^3H_4$	Γ_5	12523	12517	6	12527	12510	17	12537	12518	19
	Γ_1	12563	12567	6	12560	12569	−9	12577	12591	−14
	Γ_2	12633	12640	−7	12631	12636	−5	12646	12659	−13
	Γ_4	12662	12663	−1	12654	12653	1	12671	12677	−6
	Γ_1	12705	12705	0	1268	12686	−5	12713	12709	4
	Γ_5	12704	12710	−6	12714	12698	16	12733	12717	16
	Γ_3	12774	12784	−10	12774	12780	−6	12793	12797	−4
$^3F_3$	Γ_5	14411	14415	−4	14409	14403	6	14428	14434	−6
	Γ_3	14453	14439	14	14441	14433	8	14478	14465	13
	Γ_5	14453	14452	1	14445	14443	2		14478	
	Γ_4	14459	14458	1	14453	14446	7	14484	14478	6
	Γ_2	14475	14480	−5	14465	14473	−8	14494	14506	−12
$^3F_2$	Γ_3	15007	15009	−2	14989	14997	−8	15027	15038	−14
	Γ_1	15018	15016	2	15020	15007	13	15040	15033	7
	Γ_5	15069	15071	−2	15062	15060	2	15088	15100	−12
	Γ_4	15147	15144	3	15123	15126	−3	15184	15164	20
$^1G_4$	Γ_4	20938	20954	−16	20944	20956	−12	20946	20959	−13

TABLE I. (*Continued.*)

Multiplet	Irrep.	YVO_4			$GdVO_4$			$LuVO_4$		
		E_{exp}[a]	E_{calc}	$E_{exp}-E_{calc}$	E_{exp}	E_{calc}	$E_{exp}-E_{calc}$	E_{exp}	E_{calc}	$E_{exp}-E_{calc}$
	Γ_5	21102	21099	3	21099	21098	1	21122	21111	11
	Γ_1	21167	21164	3	21160	21155	5	21190	21189	1
	Γ_2	21234	21237	−3	21242	21231	11	21248	21254	−6
	Γ_3	21306	21307	−1	21296	21283	13	21266	21278	−12
	Γ_5		21402		21376	21386	−10	21382	21394	−12
	Γ_1	21459	21439	20	21441	21434	7	21495	21462	33
$^1D_2$	Γ_1	27736	27730	6	27734	27729	5		27746	
	Γ_5	27736	27731	4	-	27726		27739	27753	−14
	Γ_4	27753	27749	4	27754	27741	13	27782	27769	13
	Γ_3	27789	27803	−14	27773	27793	−20	27820	27820	0
$^1I_6$	Γ_3		34463			34488			34404	
	Γ_4		34491			34517			34422	
	Γ_5		34547			34561			34514	
	Γ_1		34554			34570			34525	
	Γ_3		34601			34609			34550	
	Γ_5		34727			34742			34696	
	Γ_2		34755			24766			34730	
	Γ_4		34931			34925			34864	
	Γ_5		34948			34943			34884	
	Γ_1		34959			34954			34899	
$^3P_0$	Γ_1		35138			35145			35128	
$^3P_1$	Γ_5		36116			36127			36108	
	Γ_2		36175			36178			36166	
$^3P_2$	Γ_3		37862			37860			37883	
	Γ_1		37881			37884			37888	
	Γ_5		37975			37976			38004	
	Γ_4		38154			37140			38159	

[a]Taken from. Ref. 14.

ambient. The amount of precipitates after the growth of $Tm:LuVO_4$ crystals was much greater than after the growth of $Tm:GdVO_4$ crystals. The reason why a stronger evaporation of vanadium oxide occurs in $Tm:LuVO_4$ is not clear yet. This phenomenon seems to be related to observed coloration of the grown crystals.

Absorption spectra shown in Fig. 1 are related to transitions within the $4f^{12}$ configuration of Tm^{3+} ions. Absorption lines are sharp and depend weakly on the host since the $4f$ electrons are effectively shielded by the filled $5s$ and $5p$ orbitals. In principle, three different transition mechanisms may be involved: magnetic dipole transitions, induced electric dipole transitions, and quadrupole transitions. To our knowledge the contribution of the latter mechanism to rare earth spectra has not been evidenced, however. A magnetic dipole operator has even parity. Accordingly, magnetic dipole transitions between states of the same parity (intraconfigurational transitions) are allowed in agreement with Laporte rule. The magnetic dipole matrix elements are small and in addition the selection rule $\Delta J=0, \pm 1, (0\not\leftarrow 0)$ is valid. Therefore the magnetic dipole mechanism contributes solely to the $^3H_6$-$^3H_5$ transition of Tm^{3+} at about 1200 nm. The electric dipole operator is of odd parity. Accordingly, intraconfigurational electric dipole transitions are forbidden by the Laporte rule. When a rare earth ion resides in a noncentrosymmetric site, the crystal-field Hamiltonian induces an admixture of opposite parity states (presumably those of the $5d$ configuration) to the $4f$ states. As a consequence, induced electric dipole transitions between the $^{2S+1}L_J$ multiplets belonging to the $4f^n$ configuration occur. It should be noted here that states of the $4f^n$ configuration are combinations of Russell-Saunders states, calculated in the intermediate coupling scheme. Accordingly, S and L are no longer "good" quantum numbers, but they are still used to identify states. In addition, the selection rule $\Delta S=0$ is relaxed. The crystal field splits the $^{2S+1}L_J$ multiplets giving rise to crystal-field states.

TABLE II. Hamiltonian parameters (in cm^{-1}) obtained from crystal-field (CF) analyses of Tm^{3+}-doped $GdVO_4$, YVO_4, and $LuVO_4$ single crystals. The M^k and P^k parameters were constrained by Hartree-Fock determined fixed ratios.

Parameter[a]	$Tm^{3+}:YVO_4$	$Tm^{3+}:GdVO_4$	$Tm^{3+}:LuVO_4$
E_{avg}	17857 (7)	17852 (9)	17858 (9)
F^2	101228 (26)	101275 (30)	101135 (34)
F^4	71386 (32)	71420 (35)	71154 (39)
F^6	51369 (51)	51304 (56)	51453 (63)
α	16 (3)	16 (3)	14 (3)
β	[−665]	[−665]	[−665]
γ	[1936]	[1936]	[1936]
ζ	2630 (3)	2630 (3)	2632 (4)
M^{0b}	[4.930]	[4.930]	[4.930]
P^{2b}	[893]	[893]	[893]
B_0^2	−194(14)	−168(15)	−193(17)
B_0^4	360 (18)	362 (21)	487 (23)
B_4^4	850 (14)	812 (15)	783 (17)
B_0^6	−622(19)	−639(20)	−679(23)
B_4^6	−51(14)	−8(16)	−21(18)
σ^b	11	12	13
n	48	47	44
N_v	1816	1803	1626

[a]The parameters are defined in III. Values in parentheses indicate parameter errors. Parameters in square brackets were kept constant during the fitting procedure.

[b]Standard deviation: $\sigma=\Sigma_i[(\Delta_i)^2/(n-p)]^{1/2}$ where Δ_i is the difference between the observed and calculated energies, n is the number of levels fitted, and p is the number of parameters freely varied.

In the D_{2d} site symmetry, the $2J+1$ degeneracy of multiplets of Tm^{3+} ions, which have an even number of $4f$ electrons, is not lifted completely as can be seen in Table I. The site symmetry determines also selection rules for induced electric dipole transitions and magnetic transitions between individual crystal-field levels. Those for D_{2d} symmetry are given in Table IV.

Overlapping transitions from thermally populated crystal-field levels of the ground $^3H_6$ multiplet to crystal-field levels of excited multiplets of Tm^{3+} form bands appearing in absorption spectra shown in Fig. 1. The transitions are purely electronic, there is not a Stokes shift between absorption and emission bands. Therefore, interpretation of emission spectra can be performed taking into account energies of the crystal-field levels, thermal population, and selection rules.

Absorption intensity is expressed in absorption cross-section units to facilitate the comparison of data. It follows from the spectra shown that generally π-polarized absorption bands are much narrower than σ-polarized bands and they attain significantly greater peak values. This feature is particularly apparent in the case of the $^3H_6$-$^3H_4$ band at about 800 nm in the $Tm:LuVO_4$ spectrum.

Transition intensities of Tm^{3+} in vanadates were analyzed in the framework of a theory developed independently by Judd[23] and Ofelt.[24] The theory is useful not merely in the interpretation of absorption spectra of rare earth ions but it became a powerful tool in predicting relaxation rates of excited levels. At present it is widely used to assess the laser potential of rare earth-doped materials. According to the theory, spectroscopic properties of rare earth-doped materials may be characterized by using three phenomenological parameters Ω_t $(t=2,4,6)$ which are obtained by a least-square fit between the theoretical and experimental oscillator strengths derived from absorption spectrum. Adopting this procedure, we determined experimental oscillator strengths for transitions from the ground $^3H_6$ multiplet to six excited

TABLE III. CF parameters B_m^n for $Tm^{3+}:YVO_4$ (cm^{-1}).

B_0^2	B_0^4	B_4^4	B_0^6	B_4^6	References
−132	377	898	−521	−52	14
−175	337	832	−621	−50	18
−173	341	830	−604	−55	15
−194	360	850	−622	−51	This work

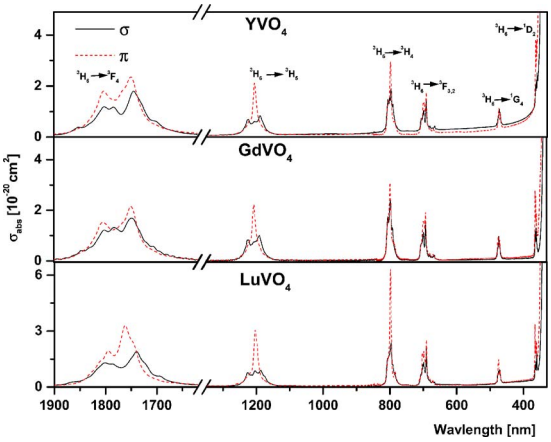

FIG. 1. (Color online) Polarized absorption cross section of Tm^{3+} in YVO_4, $GdVO_4$, and $LuVO_4$. $T=300$ K.

multiplets of Tm^{3+} by numerical integration of absorption bands presented in Fig. 1. Crystals investigated are anisotropic therefore, mean oscillator strengths P_m were evaluated according to a commonly used formula $P_m=(2P_\sigma+P_\pi)/3$ where P_σ and P_π are the oscillator strengths derived from the σ and π spectrum, respectively. For each transition the expression for theoretical oscillator strength was constructed and equated to experimental oscillator strength P_m to obtain six equations of the form

$$P_{\exp}=\frac{8\pi^2 mc}{3h\lambda(2J+1)}\frac{(n^2+2)^2}{9n}\sum_{t=2,4,6}\Omega_t|\langle f^N[L,S]J||U^{(t)}|| \times f^N[L',S']J'\rangle|^2, \quad (6)$$

where λ is the mean wavelength of the transition, n is refractive index of the host, m denotes the mass of electron, c denotes the light velocity, and h is the Planck constant. U^t are matrix elements of unit tensor operators calculated in the intermediate coupling. The matrix elements do not depend on the host, therefore their values given in Ref. 25 were used for the calculation. The Ω_t parameters have been adjusted to give the best least-square fit to the experimental oscillator strengths. In relation (6) forced electric dipole transitions are considered only. Accordingly, the contribution of the magnetic dipole transition was calculated for the $^3H_6$-$^3H_5$ transition using standard relation and subtracted calculated value from the experimental oscillator strength. Results of the fitting procedure are presented in Table V and the Ω_t parameters obtained for the three systems studied are compared in Table VI. The quality of the fit is usually expressed in terms of rms deviation defined in the preceding section. Our rms values of 6.48×10^{-7}, 7.77×10^{-7}, and 8.03×10^{-7} for $Tm:YVO_4$, $Tm:GdVO_4$, and $Tm:LuVO_4$, respectively, are comparable to those obtained in the analysis of other Tm-doped crystals.

A significantly different set of Ω_t parameters for $Tm:YVO_4$, namely $\Omega_2=13.0\times10^{-20}$ cm^2, $\Omega_4=4.74\times10^{-20}$ cm^2, and $\Omega_6=0.07\times10^{-20}$ cm^2 was reported by Chen Xueyuan and Luo Zundu.[15] However, during their least-square fit process the Ω_6 parameter was first negative. Next, a positive value of this parameter was put as a constraint condition in a subsequent fitting procedure which finally gave the set of Ω_t parameters mentioned above. It should be noted here that the incertitude of the Judd-Ofelt treatment of thulium-doped crystals is expected to be higher than that encountered in the study of neodymium or erbium-doped crystals because the Tm^{3+} absorption spectrum provides six data points only.

TABLE IV. Electric (ED) and magnetic (MD)—dipole selection rules for D_{2d} symmetry.

	ED				
D_{2d}	Γ_1	Γ_2	Γ_3	Γ_4	Γ_5
Γ_1				π	σ
Γ_2			π		σ
Γ_3		π			σ
Γ_4	π				σ
Γ_5	σ	σ	σ	σ	π
			MD		
Γ_1		σ			π
Γ_2	σ				π
Γ_3				σ	π
Γ_4			σ		π
Γ_5	π	π	π	π	σ

C. Relaxation dynamics of excited states

Having determined Ω_t parameters we calculated the rates W_r of radiative transitions from each excited multiplet to lower energy multiplets of Tm^{3+} according to the relation

$$W_r=\frac{64\pi^4 e^2}{3h\lambda^3(2J+1)}\frac{n(n^2+2)^2}{9}\sum_{t=2,4,6}\Omega_t|\langle f^N[L',S']J'||U^{(t)}|| \times f^N[L,S]J\rangle|^2. \quad (7)$$

Luminescence branching ratios β were next evaluated using the relation

$$\beta=\frac{W_r}{\sum_j W_r}. \quad (8)$$

The inverse of the rate sum of radiative transition from the given excited multiplet to an all terminal multiplet is commonly denoted as radiative lifetime τ_r of this multiplet

$$\tau_r=\frac{1}{\sum_j W_r}. \quad (9)$$

Results of calculations performed for the three systems under study are gathered in Tables VII and VIII. It can be seen in Table VIII that radiative lifetimes for all excited multiplets (except for the $^1D_2$ state) of Tm^{3+} follow a general trend, i.e., they decrease from the highest values for $Tm:YVO_4$ to the

TABLE V. Measured and calculated oscillator strengths for Tm^{3+} in YVO_4, $GdVO_4$, and $LuVO_4$.

Transition from $^3H_6$	Energy (cm^{-1})	Oscillator $\Delta P \times 10^6$				Residual $\Delta P \times 10^6$
		P_π	P_σ	P_m	P_{calc}	
			YVO_4			
$^3F_4$	5731	6.01	5.50	5.67	5.67	0.00
$^3H_5$	8336	4.12	3.41	3.21 (ed) 0.44 (md)	2.84	0.37
$^3H_4$	12590	6.41	6.05	6.17	6.25	0.08
$^3F_3+^3F_2$	14578	5.14	3.94	4.34	4.34	0.00
$^1G_4$	21195	2.89	2.62	2.71	1.79	0.92
$^1D_2$	27573	5.73	3,.51	4.25	3.73	0.52
			$GdVO_4$			
$^3F_4$	5671	6.76	6.29	6.45	6.45	0.00
$^3H_5$	8308	4.10	4.06	3.64 (ed) 0.44 (md)	3.39	0.25
$^3H_4$	12589	7.43	6.98	7.13	7.13	0.00
$^3F_3+^3F_2$	14635	6.80	4.99	5.60	5.60	0.00
$^1G_4$	21203	3.46	3.35	3.39	2.07	1.32
$^1D_2$	27651	7.18	409	5.12	4.72	2.00
			$LuVO_4$			
$^3F_4$	5679	8.10	6.55	7.06	7.06	0.00
$^3H_5$	8356	5.62	4.17	4.21 (ed) 0.44 (md)	4.06	0.15
$^3H_4$	12604	7.56	7.38	7.44	8.05	0.61
$^3F_3+^3F_2$	14542	8.55	6.58	7.24	7.24	0.00
$^1G_4$	21217	3.95	3.28	3.50	2.26	0.45
$^1D_2$	27591	5.38	3.23	3.95	3.95	0.00

lowest values for $Tm:LuVO_4$. It may be interesting to note here that Chen Xueyuan and Luo Zundu[15] obtained very similar radiative lifetimes τ_{rad} amounting to 1165 and 262 μs for the $^3F_4$ and $^3H_4$ multiplets of Tm^{3+} in YVO_4 using significantly different set of Ω_t parameters mentioned above.

Luminescence lifetimes of the $^1G_4$, $^3H_4$, and $^3F_4$ of Tm^{3+} in YVO_4, $GdVO_4$, and $LuVO_4$ were derived from luminescence decay curves recorded at room temperature. In this measurement the $^1G_4$ and $^3H_4$ multiplets were excited directly, whereas the excitation of the $^3F_4$ multiplet was made through the $^3H_4$ or $^3H_5$ levels. Results of the measurement are gathered in Table IX. The consistence of the Judd-Ofelt treatment can be checked with lifetime data recorded for samples with low Tm^{3+} concentration since in heavy-doped samples the self-quenching of luminescence occurs. Diluted $Tm:GdVO_4$ and $Tm:LuVO_4$ samples are not available, accordingly the experimental lifetimes recorded for YVO_4 containing 0.5% of Tm^{3+} can be used for this purpose. It can be seen that experimental and calculated radiative lifetimes of the $^1G_4$ and $^3H_4$ multiplets are in reasonable agreement. When the Tm^{3+} concentration is higher the self-quenching phenomenon involving the cross-relaxation process shortens these lifetimes in the three systems with comparable efficiencies. The cross-relaxation process $^3H_4+^3H_6 \rightarrow {}^3F_4+{}^3F_4$ is particularly important since it transfers the excitation from the $^3H_4$ pump level to the $^3F_4$ upper laser level thus providing a so-called "two-for-one pumping."

TABLE VI. The Judd-Ofelt parameters for Tm^{3+} in YVO_4, $GdVO_4$, and $LuVO_4$.

	Ω_2 (10^{-20} cm^2)	Ω_4 (10^{-20} cm^2)	Ω_6 (10^{-20} cm^2)
YVO_4	7.81	1.03	1.14
$GdVO_4$	8.13	1.45	1.35
$LuVO_4$	8.44	1.82	1.78

There is however, significant disagreement between calculated radiative lifetimes and corresponding experimental lifetimes for the $^3F_4$ level, at least in the case of the $Tm:YVO_4$ and $Tm:GdVO_4$. The luminescence lifetimes measured are two times higher roughly than calculated radiative lifetimes. It is well known that the measurement of luminescence lifetimes should be performed carefully taking into account the phenomenon of self-absorption, particularly in the case of first excited states that decay exclusively by direct transitions to the ground state. Self-absorption, if present, tends to lengthen the measured lifetime. To avoid this phenomenon thin samples were used. In addition, several samples were ground to obtain fine powder and next

TABLE VII. Calculated values of the radiative transition rates W_r for excited states of Tm^{3+} in YVO_4, $GdVO_4$, and $LuVO_4$.

		Averange wave number (cm^{-1})			Wr (s^{-1})		
SLJ	S′L′J′	YVO_4	$GdVO_4$	$LuVO_4$	YVO_4	$GdVO_4$	$LuVO_4$
$^3F_4$	$^3H_6$	5731	5670	5678	828	965	1060
$^3H_5$	$^3F_4$	2604	2637	2677	93	113	125
	$^3H_6$	8336	8308	8356	718	892	1079
$^3H_4$	$^3H_5$	4254	4280	4248	188	229	251
	$^3F_4$	6858	6918	6925	163	246	303
	$^3H_6$	12589	12589	12604	4402	5259	5950
$^3F_{3,2}$	$^3H_4$	1989	2046	1937	22	28	26
	$^3H_5$	6243	6327	6185	919	1290	1324
	$^3F_4$	8847	8964	8863	819	1542	1599
	$^3H_6$	14578	14635	14541	4009	4564	5826
$^1G_4$	$^3F_{3,2}$	6616	6567	6675	225	234	306
	$^3H_4$	8605	8614	8612	548	1115	1248
	$^3H_5$	12859	12895	12860	1306	2756	3255
	$^3F_4$	15463	15532	15538	378	468	596
	$^3H_6$	21195	21203	21216	3857	4329	4735
$^1D_2$	$^1G_4$	6387	6448	6374	784	797	823
	$^3F_{3,2}$	13005	13016	13049	8721	8651	9484
	$^3H_4$	15011	15062	14987	26814	26790	27610
	$^3H_5$	19298	19343	19235	353	318	410
	$^3F_4$	21953	21980	21912	24654	23354	25561
	$^3H_6$	27612	27651	27590	20114	19964	25165

measured. In powdered samples a thin surface layer was excited. In our opinion a disagreement between calculated radiative lifetimes and experimental luminescence lifetimes of the $^3F_4$ level cannot be explained by a lengthening effect due to self-absorption. Our conclusion is corroborated by following observations: (i) lifetimes recorded for samples with higher Tm^{3+} concentrations are shorter, whereas self-absorption phenomenon implies contrary dependence; (ii) the $^3F_4$ lifetimes measured for $Tm:LuVO_4$ samples in identical conditions and sample geometry are significantly shorter. Figure 2 compares luminescence decay curves for the three systems containing a similar concentration of Tm^{3+}. Our experimental $^3F_4$ lifetimes for the $Tm:GdVO_4$ samples are consistent with corresponding experimental data reported by Higuchi *et al.*,[17] but lifetimes for the $Tm:LuVO_4$ crystal are not yet reported, as far as we know. To account for these findings the $^3F_4$ radiative lifetimes were recalculated using a relation

$$W_r = \frac{8\pi^2 e^2 n^2}{mc\lambda^2} \frac{(2J+1)}{(2J'+1)} \cdot P_{\exp}, \tag{10}$$

where $P_{\exp}$ is experimental oscillator strength, m denotes mass of electron, c denotes the light velocity, e is electron charge, λ is the mean wavelength of the transition, and h is the Planck constant. Inserting values of experimental oscillator strengths for the $^3H_6$-$^3F_4$ transition from Table III the $^3F_4$ radiative lifetimes amounting to 2.58, 2.25, and 2.06 ms were obtained for the $Tm:YVO_4$, $Tm:GdVO_4$, and $Tm:LuVO_4$, respectively. Thus, it appears that the $^3F_4$ radiative transition rates evaluated by the Judd-Ofelt treatment are significantly overestimated. If so, the question arises as to why the experimental $^3F_4$ lifetimes for the $Tm:LuVO_4$ are shorter. One possible explanation is the migration accelerated energy transfer to unintentional sinks. Measurements of the $^3F_4$ lifetime for $LuVO_4$ crystals containing low Tm^{3+} concentration may be informative but such samples are not available. Accordingly, this problem remains open and waits for explanation.

D. Analysis of spectra relevant to laser performance

Knowledge on shape, anisotropy, and spectral positions of pump bands as well as on the dependence of emission cross section on wavelength and light polarization is essential for an assessment of laser performance of an active material. Based upon these data the geometry of laser active element as well as the configuration of optical pumping and resonator can be optimized. Relevant features of the pump bands, associated with the $^3H_6$-$^3H_4$ transition of Tm^{3+} in the three systems under study are shown in Fig. 3. The bands are rather structureless and broad as a consequence of important

TABLE VIII. Calculated values of branching ratios β and total radiative lifetimes τ_{rad} for excited states of Tm^{3+} in YVO_4, $GdVO_4$, and $LuVO_4$.

		β			τ_{rad} (μs)		
SLJ	S′L′J′	YVO_4	$GdVO_4$	$LuVO_4$	YVO_4	$GdVO_4$	$LuVO_4$
$^3F_4$	$^3H_6$	1	1	1	1208	1036	943
$^3H_5$	$^3F_4$	0.12	0.11	0.10	1237	996	831
	$^3H_6$	0.88	0.89	0.90			
$^3H_4$	$^3H_5$	0.04	0.04	0.04	224	174	154
	$^3F_4$	0.03	0.04	0.05			
	$^3H_6$	0.93	0.92	0.91			
$^3F_{3,2}$	$^3H_4$	0.00	0.00	0.00	175	135	114
	$^3H_5$	0.16	0.17	0.15			
	$^3F_4$	0.14	0.21	0.18			
	$^3H_6$	0.70	0.61	0.66			
$^1G_4$	$^3F_{3,2}$	0.04	0.03	0.03	137	112	99
	$^3H_4$	0.09	0.13	0.12			
	$^3H_5$	0.21	0.31	0.32			
	$^3F_4$	0.06	0.05	0.05			
	$^3H_6$	0.61	0.49	0.47			
$^1D_2$	$^1G_4$	0.00	0.00	0.00	12	13	11
	$^3F_{3,2}$	0.12	0.11	0.11			
	$^3H_4$	0.29	0.34	0.31			
	$^3H_5$	0.02	0.01	0.01			
	$^3F_4$	0.28	0.29	0.29			
	$^3H_6$	0.29	0.25	0.28			

electron-phonon coupling. This is highly advantageous for optical pumping with laser diodes because the stringent control of a laser diode temperature is not needed.

One of the most important parameters influencing the laser performance of the material is the stimulated emission cross section. In the simplest approach it can be determined by a so-called reciprocity method, which is based on the relation between the absorption cross section σ_{abs} and emission cross section σ_{em}:

$$\sigma_{em}(\lambda) = \frac{Z_{low}}{Z_{up}}\sigma_a(\lambda)\exp\left(\frac{E_{ZL} - E(\lambda)}{k_B T}\right), \tag{11}$$

where λ is the wavelength, T is temperature, and E_{ZL} denotes the energy difference between the lowest crystal-field component of the ground multiplet and the lowest crystal-field component of the excited multiplet. Z_{low} and Z_{up} are partition functions for lower and upper multiplets, respectively, evaluated according to the formula

$$Z_{low} = \sum_{i=1}^{n} g_i \exp\left(\frac{-E_i}{k_B T}\right), \quad Z_{up} = \sum_{j=1}^{n} g_j \exp\left(\frac{-[E_j - E(\lambda)]}{k_B T}\right). \tag{12}$$

To make use of this approach, the room temperature absorption spectrum and energies of the crystal-field components of

TABLE IX. Measured lifetimes of $^3F_4$, $^3H_4$, and $^1G_4$ excited states of Tm^{3+} in YVO_4, $GdVO_4$, $LuVO_4$.

Crystal	$^3F_4$ (ms)	$^3H_4$ (μs)	$^1G_4$ (μs)
Tm (0.5 at. %) YVO_4	1.9	176	101
Tm (6 at. %) YVO_4	1.4	7	8
Tm (2 at. %) $GdVO_4$	1.9	52	57
Tm (4 at. %) $GdVO_4$	1.8	18	15
Tm (6 at. %) $GdVO_4$	1.2	8	4
Tm (3 at. %) $LuVO_4$	0.57	12	23
Tm (5 at. %) $LuVO_4$	0.32	6	8

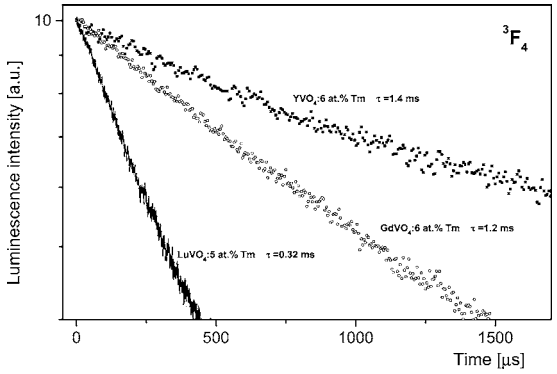

FIG. 2. Decay curves of the $^3F_4$ luminescence collected from YVO_4:Tm (6 at. %), $GdVO_4$:Tm (6 at. %), and $LuVO_4$:Tm (5 at. %) single crystals at room temperature.

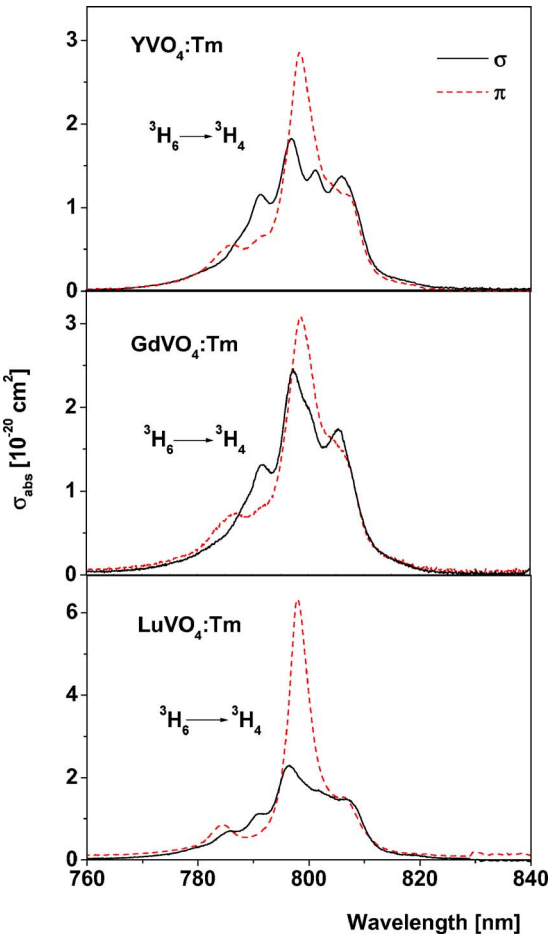

FIG. 3. (Color online) Polarized absorption cross section corresponding to the $^3H_6$-$^3H_4$ transition of Tm^{3+} ions in the YVO_4, $GdVO_4$, and $LuVO_4$ crystals.

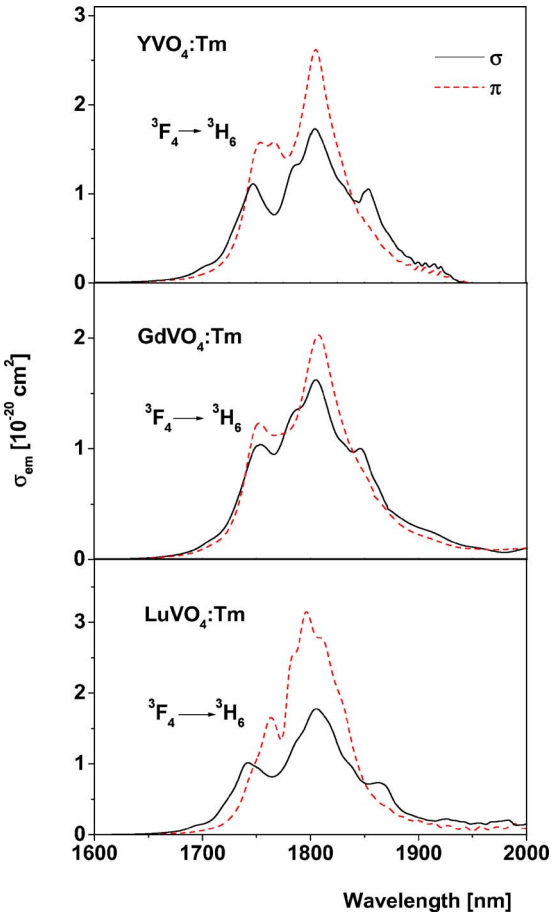

FIG. 4. (Color online) Calculated polarized emission cross section corresponding to the $^3F_4$-$^3H_6$ transition of Tm^{3+} in the YVO_4, $GdVO_4$, and $LuVO_4$ systems.

multiplets involved are needed. The stimulated emission cross section as a function of wavelengths has been calculated for materials under study using the $^3H_6$-$^3F_4$ absorption bands shown in Fig. 1 and experimental energies of the crystal-field levels of the $^3H_6$ and $^3F_4$ multiplets given in Table I. Missing experimental data points for the ground $^3H_6$ multiplet were substituted by those calculated. In Fig. 4 the stimulated emission cross sections $\sigma_{em}(\lambda)$ for π and σ polarization are compared. Anisotropy of the $^3F_4$-$^3H_6$ emission band for $Tm:LuVO_4$ is particularly strong and the peak value of emission cross section for π polarization is the highest as compared to two remaining systems. However, effective emission cross sections will be smaller due to the reabsorption. Reabsorption losses are expected to be significant because of a relatively small splitting of the ground state of Tm^{3+} in vanadate crystals. To account for this factor the effective emission cross sections $\sigma_{\text{eff}}(\lambda)$ were calculated according to the relation

$$\sigma_{eff}(\lambda) = [P\sigma_{em}(\lambda) - (1-P)\sigma_a(\lambda)], \tag{13}$$

where P is a population inversion parameter defined as the ratio of the number of ions in the upper laser level to the total number of active ions. Results of the calculation for several reasonable values of P are shown in Figs. 5 and 6. It can be seen that in spite of relatively small ground state splitting, positive values of effective emission cross sections are obtained. Based upon these results the wavelength tunability range of the laser emission between about 1825 and 1950 nm can be predicted. Reported generation wavelengths of the $Tm:YVO_4$ laser, namely 1870 nm (Ref. 8) and 1940 nm (Ref. 7) as well as the generation wavelength of 1940 nm reported for the $Tm:GdVO_4$ laser are in good agreement with the calculated data. It should be remembered however, that the effective emission cross section was derived from the wing of the absorption spectrum where the signal-to-noise ratio is small. Accordingly, the results shown may be considered as rough estimates.

E. Laser performance of $Tm:GdVO_4$ and $Tm:LuVO_4$

To underpin the importance of a thorough spectroscopic study of thulium-doped vanadate materials, laser performance of different floating-zone-grown crystals $Tm:GdVO_4$ and $Tm:LuVO_4$ was examined. Several $Tm:GdVO_4$ and $Tm:LuVO_4$ crystal samples of variable Tm^{3+} concentrations spanning from 2 to 6 at. % were examined under diode pumping. A fiber-coupled pumping diode (HLU20F400—LIMO Laser Systems) with fiber output power of up to 17 W

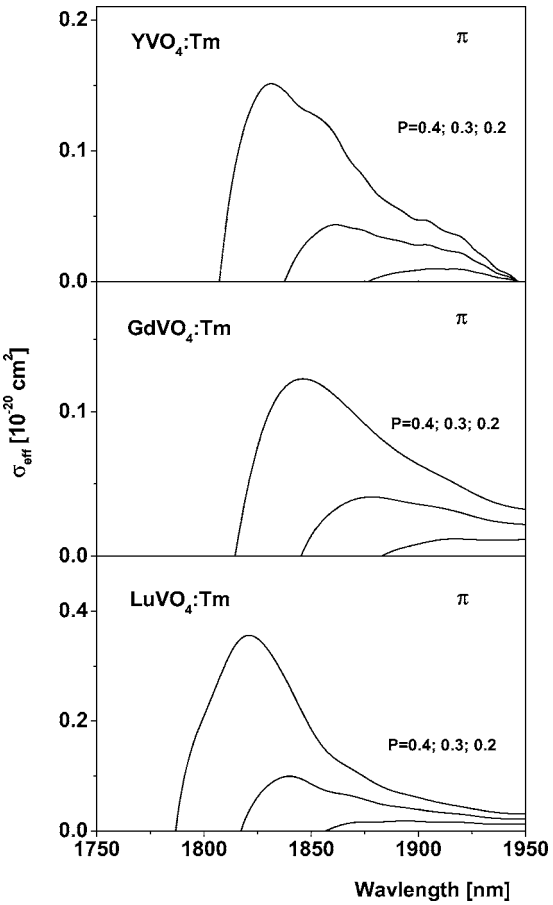

FIG. 5. Calculated effective cross section for π polarization corresponding to the ${}^3F_4$-${}^3H_6$ transition Tm^{3+} in the YVO_4, $GdVO_4$, and $LuVO_4$ crystals for several P parameters.

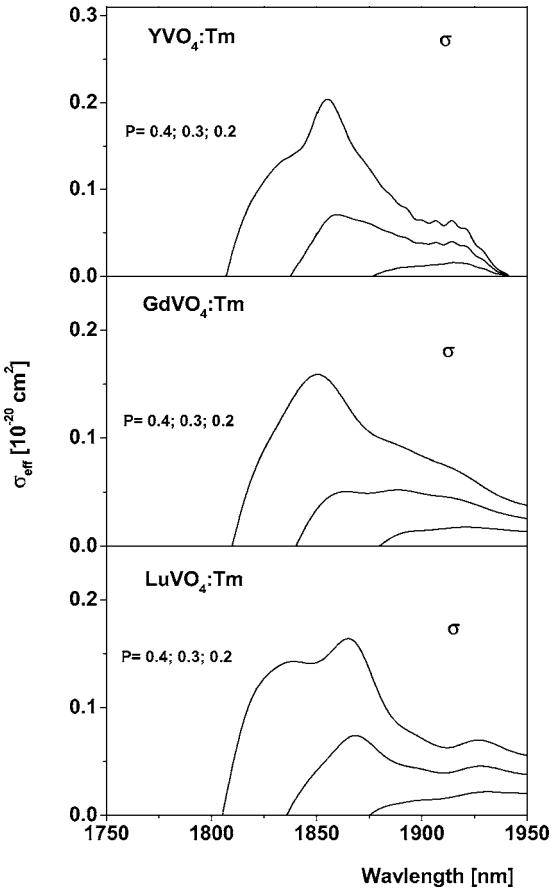

FIG. 6. Calculated effective cross section for σ polarization corresponding to the ${}^3F_4$-${}^3H_6$ transition Tm^{3+} in the YVO_4, $GdVO_4$, and $LuVO_4$ crystals for several P parameters.

at 808 nm was used. A linear two-mirror resonator was constructed using a flat mirror highly reflective at ≈ 2 μm and a curved output coupler with the radius of curvature of ≈ 150 mm. The resonator length was 35 mm and the pumping beam focus was ≈ 360 μm. The antireflection-coated $Tm:GdVO_4$ sample was clamped in a water-cooled copper block and was placed centrally between the mirrors. The free running operation of the $Tm:GdVO_4$ laser was centered at 1910 nm. Figure 7 shows output power recorded as a function of absorbed pump power for the $Tm:GdVO_4$ (Tm^{3+} concentration 4 at. %) laser operating in the cw mode. A laser operated with a slope efficiency of 39.5% with respect to the absorbed power and a maximum output of 2.6 W was

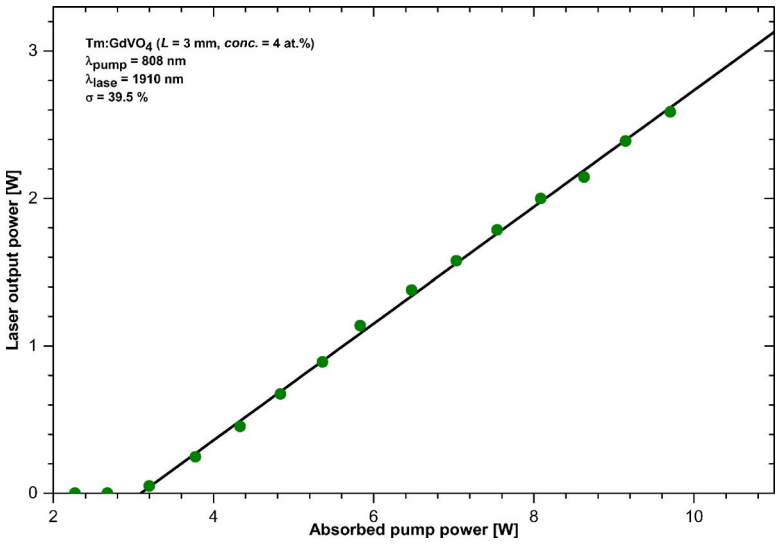

FIG. 7. (Color online) Output power recorded as a function of absorbed pump power for the $Tm:GdVO_4$ ${}^3F_4$-${}^3H_6$ laser operating in the cw mode.

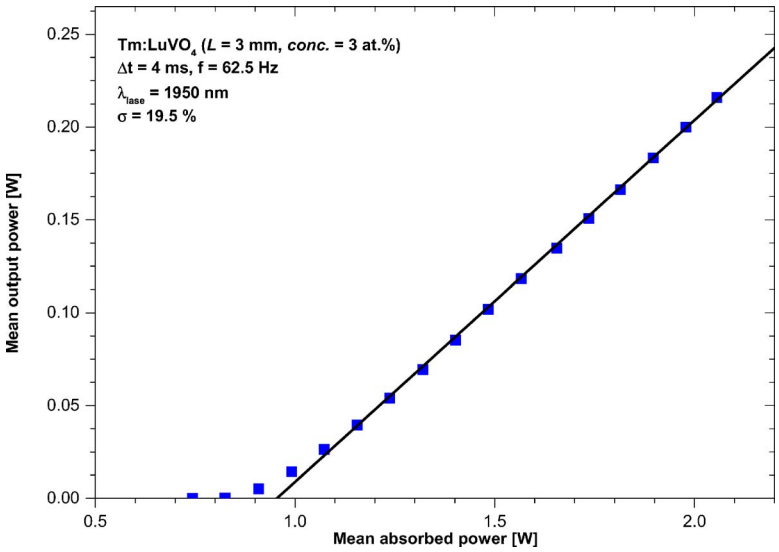

FIG. 8. (Color online) Output power recorded as a function of absorbed pump power for the $Tm:LuVO_4$ $^3F_4$-$^3H_6$ laser operating in the quasi-cw mode.

obtained, only limited by the available pump power. Our study confirms that thulium-doped gadolinium vanadate is a highly efficient laser material especially when the improved sample quality is obtained utilizing floating-zone growth.

In the same conditions the cw laser operation of $Tm:LuVO_4$ was not achieved, however. In a pulsed mode a maximum average output power of 210 mW was obtained with a Tm^{3+} concentration of 2 at. %. Pump pulses were 4 ms at 25% duty cycle. The $Tm:LuVO_4$ laser was emitted at 1950 nm. The corresponding input-output characteristic is shown in Fig. 8. The slope efficiency of about 19.5% was estimated, a value significantly inferior to that recorded for the $Tm:GdVO_4$ laser. We believe that with the improvement of material quality and optimization of laser a conditions, a continuous wave operation of $Tm:LuVO_4$ can be achieved. Our preliminary results suggest that thermally related quenching is responsible for a diminished laser performance of this different material.

IV. CONCLUSIONS

An investigation furnished the information on fundamental optical properties of thulium-doped YVO_4, $GdVO_4$, and $LuVO_4$ single crystals and made it possible to compare the basic material parameters. Crystal-field analysis provided the missing energies of the crystal-field levels for the ground $^3H_6$ multiplet of thulium ions. The overall $^3H_6$ splitting evaluated is relatively small and weakly influenced by the host. The calculated radiative lifetimes of thulium luminescent levels follow a general trend diminishing in agreement with the sequence: $YVO_4:Tm^{3+} \rightarrow GdVO_4:Tm^{3+} \rightarrow LuVO_4:Tm^{3+}$. Luminescence lifetimes measured for the systems under study are similar except for the $^3F_4$ lifetime, which appears to be surprisingly short for $LuVO_4:Tm^{3+}$. The anisotropy of absorption spectra is particularly pronounced in $LuVO_4:Tm^{3+}$. The peak absorption cross section for the band relevant for optical pumping at about 805 nm is roughly three times higher for π polarization. Also, the $LuVO_4:Tm^{3+}$ has the highest peak value of a stimulated emission cross section for the $^3F_4$-$^3H_6$ transition near 1800 nm. A multiwatt cw laser operation in $GdVO_4:Tm^{3+}$ with a slope efficiency exceeding 39% is demonstrated. In $LuVO_4:Tm^{3+}$ the cw laser operation was not achieved but the laser oscillation in a quasi-cw mode was observed.

From the inspection of data gathered in this work it can be concluded that differences between material spectroscopic parameters relevant for laser operation in the three systems are rather small. Accordingly, in the choice of the best laser crystal the physicochemical properties such as thermal conductivity and thermal expansion coefficient would be of greater importance. The major reason for the inferior laser performance of $LuVO_4:Tm^{3+}$ is thermal loading resulting from a low quantum efficiency of the $^3F_4$ upper laser level. The origin of the luminescence quenching mechanism involved is not clear and waits for explanation.

ACKNOWLEDGMENT

This work was supported by The Polish Committee for Scientific Research (2005–2007).

*Corresponding author. Fax: (4871) 344 10 29; Electronic address: R.Lisiecki@int.pan.wroc.pl

[1] I. R. O'Connor, Appl. Phys. Lett. **9**, 407 (1966).
[2] G. E. Venikouas and R. C. Powell, J. Lumin. **16**, 29 (1978).
[3] J. A. Capobianco, P. Kabro, F. S. Ermeneux, R. Moncorge, M. Bettinelli, and E. Cavalli, Chem. Phys. **214**, 329 (1997).
[4] F. S. Ermeneux, C. Goutaudier, R. Moncorge, Y. Sun, R. L. Cone, E. Zannoni, Cavalli, and M. Bettinelli, Phys. Rev. B **61**, 3915 (2000).
[5] P. Le Boulanger, J. L. Doualan, S. Girard, J. Margerie, and R.

Moncorge, Phys. Rev. B **60**, 11380 (1999).
[6] W. Ryba-Romanowski, P. Solarz, G. Dominiak-Dzik, R. Lisiecki, and T. Łukasiewicz, Laser Phys. **14**, 250 (2004).
[7] Kei Ohta, Hideaki Saito, and Minoru Obara, J. Appl. Phys. **73**, 3149 (1993).
[8] C. Hauglie-Hanssen, S. Chaddha, L. B. Shaw, R. S. F. Chang, N. Djeu, and H. Saito, *Technical Digest on CLEO '92* , Anaheim 1992, Paper No. CMD4 (Optical Society of America, Washington, DC, 1992).
[9] V. A. Mikhailov, Yu. D. Zavartsev, A. I. Zagumenyi, V. G. Ostroumov, P. A. Studenikin, E. Heumann, G. Huber, and I. Shcherbakov, Quantum Electron. **27**, 13 (1997).
[10] C. P. Wyss, W. Lüthy, H. P. Weber, V. L. Valsov, Yu. D. Zavartsev, A. I. Zagumenyi, P. A. Studenikin, and I. Shcherbakov, Appl. Phys. B **67**, 545 (1998).
[11] C. P. Wyss, W. Lüthy, H. P. Weber, V. L. Valsov, Yu. D. Zavartsev, A. I. Zagumenyi, P. A. Studenikin, and I. Shcherbakov, Opt. Commun. **153**, 63 (1998).
[12] Yoshiharu Urata and Satoshi Wada, Appl. Opt. **44**, 3087 (2005).
[13] M. Higuchi, T. Shimizu, J. Takahashi, T. Ogawa, Y. Urata, T. Miura, S. Wada, and H. Machida, J. Cryst. Growth **283**, 100 (2005).
[14] K. D. Knoll, Phys. Status Solidi B **45**, 553 (1971).
[15] Chen Xueyuan and Luo Zundu, J. Phys.: Condens. Matter **9**, 7981 (1997).
[16] R. Lisiecki, P. Solarz, G. Dominiak-Dzik, W. Ryba-Romanowski, and T. Łukasiewicz, Laser Phys. **16**, 303 (2006).
[17] M. Higuchi, K. Kodaira, Y. Urata, S. Wada, and H. Machida, J. Cryst. Growth **265**, 487 (2004).
[18] D. E. Wortman, R. P. Leavitt, and C. A. Morrison, J. Phys. Chem. Solids **35**, 591 (1974).
[19] M. C. Favas and D. L. Kepert, Prog. Inorg. Chem. **26**, 325 (1980).
[20] C. Linares, A. Louat, and M. Blanchard, Struct. Bonding (Berlin) **33**, 179 (1977).
[21] C. Brecher, H. Samelson, A. Lempicki, R. Riley, and T. Peters, Phys. Rev. **155**, 178 (1967).
[22] C. Görller-Walrand and K. Binnemans, *Handbook on the Physics and Chemistry of Rare Earths*, edited by K. A. Gschneider, Jr. and L. Eyring(Elsevier, Amsterdam, 1996), Vol. 23, p. 121.
[23] B. R. Judd, Phys. Rev. **127**, 750 (1962).
[24] G. S. Ofelt, J. Chem. Phys. **37**, 511 (1962).
[25] A. A. Kaminski, *Crystalline Lasers, Physical Processes and Operating Schemes* (CRC, Boca Raton, FL, 1996).